Available online at www.sciencedirect.com
SCIENCE DIRECT®
Tectonophysics 407 (2005) 211–225
TECTONOPHYSICS
www.elsevier.com/locate/tecto

Deformation of oceanic lithosphere near slow-spreading ridge discontinuities

J.W. van Wijk *, D.K. Blackman

IGPP, Scripps Institution of Oceanography, UCSD, La Jolla CA 92093-0225, USA

Received 7 September 2004; received in revised form 2 June 2005; accepted 5 August 2005

Abstract

Transform and non-transform discontinuities that offset slow spreading mid-ocean ridges involve complex thermal and mechanical interactions. The truncation of the ridge axis influences the dynamics of spreading and accretion over a certain distance from the segment-end. Likewise, the spreading system is expected to influence the lithospheric plate adjacent to the ridge-end opposite of the discontinuity. Tectonic effects of the truncated ridge are noticeable in for example the contrast between seafloor topography at inside corners and outside corners, along-axis variations in rift valley depth, style of crustal accretion, and ridge segment retreat and lengthening. Along such slow-spreading discontinuities and their fossil traces, oceanic core complexes or mega-mullion structures are rather common extensional tectonic features. In an attempt to understand deformation of oceanic lithosphere near ridge offsets, the evolution of discontinuities, and conditions that may favor oceanic core complex formation, a three-dimensional thermo-mechanical model has been developed. The numerical approach allows for a more complete assessment of lithosphere deformation and associated stress fields in inside corners than was possible in previous 3-D models. The initial suite of results reported here focuses on deformation when axial properties do not vary along-strike or with time, showing the extent to which plate boundary geometry alone can influence deformation. We find that non-transform discontinuities are represented by a wide, oblique deformation zone that tends to change orientation with time to become more parallel to the ridge segments. This contrasts with predicted deformation near transform discontinuities, where initial orientation is maintained in time. The boundary between the plates is found to be vertical in the center of the offset and curved at depth in the inside corners near the ridge–transform intersection. Ridge–normal tensile stresses concentrate in line with the ridge tip, extending onto the older plate across the discontinuity, and high stress amplitudes are absent in the inside corners during the magmatic accretionary phase simulated by our models. With the tested rheology and boundary conditions, inside corner formation of oceanic core complexes is predicted to be unlikely during magmatic spreading phases. Additional modeling studies are needed for a full understanding of extensional stress release in relatively young oceanic lithosphere.

Keywords: Mid-ocean ridge; Slow-spreading ridge; Lithosphere deformation; Numerical model; Oceanic core complex

1. Introduction

Slow and ultraslow spreading mid-ocean ridges comprise about half of the global ridge system. Plate separation at these ridge axes is not always accommodated by magmatic processes; episodes of magmatic and amagmatic phases alternate (Macdonald, 1986; Lagabrielle et al., 1998). Diverse geological and geophysical observations reveal a ridge partitioning into segments bounded by discontinuities of different type. Slow spreading ridges are offset every

* Corresponding author.
E-mail address: jvanwijk@ucsd.edu (J.W. van Wijk).

0040-1951/$ - see front matter © 2005 Elsevier B.V. All rights reserved.
doi:10.1016/j.tecto.2005.08.009

~10 to ~100 km by transform (first-order) and non-transform (second-order) discontinuities (Fig. 1). Non-transform or second-order discontinuities are associated with a relatively wide deformation zone with complex morphology and tectonics, and they have limited life span (Grindlay et al., 1991). First-order or transform offsets represent a plate boundary along which deformation is focused over a narrow zone of strike-slip faulting. They generally offset the ridge by a large distance (>30 km) and age (>1 My), and are oriented in the direction of relative plate motion. The trace of transform offsets can extend thousands of km away from the axis (Menard and Atwater, 1968). Slow-spreading ridge segmentation is likely the result of a combination of factors. Structures inherited from pre-breakup continental rifting, spreading rate and (a-)symmetry, history of the pole of opening, and mantle processes have all been suggested to play a role in the origin and evolution of these discontinuities (e.g., Grindlay et al., 1991). It has been documented that non-transform discontinuities sometimes evolve from transform discontinuities (Grindlay et al., 1991), and that offset lengths of both transform and non-transform discontinuities may vary in time (e.g., Carbotte et al., 1991; Sempéré et al., 1995). Many ridge segments have a history in which the location of the discontinuity has shifted in time, through retreat of one of the ridge segments and lengthening of the other segment (e.g., Carbotte et al., 1991; Grindlay et al., 1991; Sempéré et al., 1995; Lonsdale, 1994). Both first and second-order discontinuities thus seem to constantly evolve.

This study focuses on deformation of young oceanic lithosphere near slow-spreading ridge discontinuities and implications for the evolution of such discontinuities. At a ridge–discontinuity intersection, a relatively cold edge of lithosphere is juxtaposed against the truncated axis of accretion. Depending on factors like offset length, mechanical coupling of the contingent transform fault, and spreading velocity, i.e., the thermal structure, strength and rheological properties of the lithosphere, (e.g., Carbotte et al., 1991; Lonsdale, 1994) this truncation of the ridge axis will influence the dynamics of spreading and accretion, and thus the geologic structure of the lithosphere, over a certain distance from the segment-end. Likewise, the spreading system is expected to influence the lithospheric plate adjacent to the ridge-end opposite of the discontinuity. This tectonic interaction between the ridge axis and offsets is most evident in the contrast between seafloor topography at inside corners and outside corners (Tucholke and Lin, 1994), Fig. 1, along-axis variations in rift valley depth, magmatic properties and crustal thickness (Karson and Dick, 1983; Tolstoy et al., 1993; Tucholke and Lin, 1994; Blackman et al., 1998), distribution of earthquakes (Smith et al., 2003), and documentations of segment retreat and lengthening.

An explanation suggested for the rather consistent asymmetry between inside corner and outside corner tectonic settings is that it periodically develops by deformation along detachment faults (Tucholke and Lin, 1994; Karson, 1990; Dick et al., 1981). Inside corners would then be formed by the footwalls and

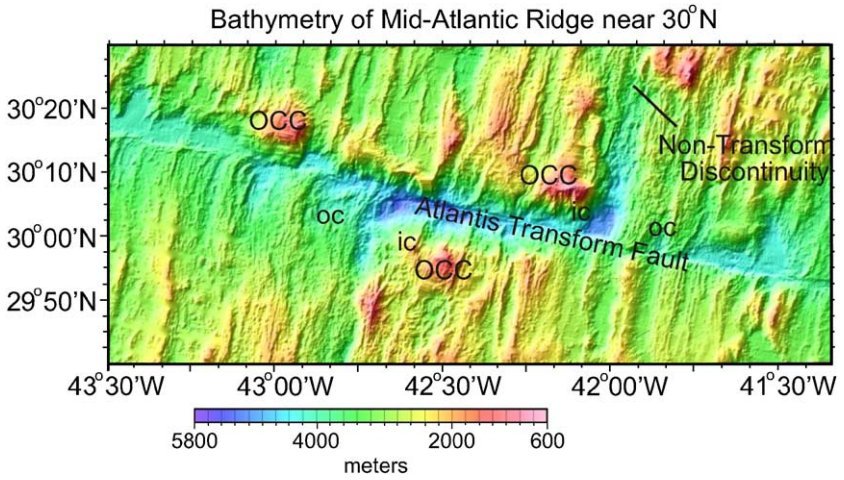

Fig. 1. Bathymetry map of the Mid-Atlantic Ridge system near 30°N. SeaBeam 2000 data collected during the MARVEL2000 cruise have been added to the compilation in Blackman et al. (1998). The slow-spreading ridge is offset by both first-order discontinuities (Atlantis Transform) and second-order or non-transform discontinuities. Inside corners (ic) are elevated with respect to outside corners (oc). Oceanic metamorphic core complexes (OCC) are present near the Atlantis Transform and its passive trace.

outside corners by hanging walls, in a similar way to Basin and Range style extension by slip along detachment faults (e.g., Davis and Lister, 1988; Lister and Davis, 1989; Wernicke, 1985, 1992, 1995). It has been suggested (e.g., Karson, 1990; Tucholke and Lin, 1994) that oceanic core complexes (OCC) are formed by slip along detachment faults rooting below the rift valley. OCC or mega-mullion structures are a rather common tectonic feature on slow spreading ridge flanks. The core or mega-mullion is an abnormally elevated, dome-like structure comprising unroofed, deformed lower crustal and upper mantle rocks (Cann et al., 1997; Dick et al., 2000; MacLeod et al., 2002; Tucholke et al., 1998). The domal cores are elevated 0.5–2.0 km above surrounding seafloor, and extend parallel to plate flow lines about 10–20 km, and in the along-strike direction from 15–40 km. Their surfaces display corrugations and striations oriented parallel to the plate spreading direction (Cann et al., 1997; Searle et al., 2003). They are characterized by positive Mantle Bouguer anomalies. Sampled structures show outcrop of serpentinized peridotites and gabbro (e.g., Blackman et al., 1998, 2002; Dick et al., 1991, 2000; Mével et al., 1991; Escartín et al., 2003). There is debate about when during the ocean spreading process the detachment system is active (only during amagmatic phases, (Tucholke et al., 1998), during magmatic phases (Dick et al., 2000), or during both (Escartín et al., 2003)), and debate about the depth of detachment fault rooting, and its dip angle at larger depths (Escartín et al., 2003). The fact that OCC are most common near ridge discontinuities, or traces of discontinuities in older lithosphere, suggests that processes that typically occur near the ridge truncation play a role in their origin.

In order to determine how plate boundary geometry contributes to processes of young oceanic lithosphere deformation, we simulate deformation near slow-spreading segment discontinuities with a finite element model. In a ridge–discontinuity–ridge setting, influences of offset length, offset nature (i.e., transform fault or second-order discontinuity) and along-axis variations in crustal structure on lithosphere deformation are studied. In our modeling approach, 3-D lithosphere deformation is explicitly predicted and the tie between asthenosphere and lithosphere is self-consistent. The chosen approach is designed to facilitate studying the relation between axial behavior and the predicted stress fields at inside corners and near ridge offsets. In this study we prescribe axial properties that would be appropriate during a magmatic accretionary phase, with no along-axis variation. This provides a useful reference for future numerical studies where axial properties will be varied in time and along-strike.

2. Models of a slow-spreading segmented ridge

Lithosphere deformation near a segment discontinuity is controlled by the forces or stresses acting upon the lithosphere and its rheological properties. These stresses result from a combination of factors, such as cooling of the lithosphere, ridge discontinuity or plate boundary geometry, asthenospheric flow, and (far field) forces transmitted through the lithosphere. In order to examine numerically lithosphere deformation near segment ends, it is thus important to describe the three-dimensional flow and thermal structure in the model simulations. In this study the problem is approached using a thermo-mechanical model that incorporates non-linear temperature dependent rheology, and brittle faulting at shallow depths. Previous 3-D numerical modeling studies chose a different approach in studying ridge discontinuity dynamics and for example did not include lithosphere deformation (e.g., Shen and Forsyth, 1992; Sparks et al., 1993), or focused on different aspects, like the thermal structure of the lithosphere (e.g., Forsyth and Wilson, 1984), or did not include viscous asthenospheric contributions (e.g., Behn et al., 2002; Fujita and Sleep, 1978; Grindlay and Fox, 1993; Phipps Morgan and Parmentier, 1984), or chose a different description for spreading axis behavior (Furlong et al., 2001).

2.1. Numerical approach

The finite element code used in this study consists of a mechanical and a thermal part. The mechanical part is based on Tekton (Melosh and Raefsky, 1980, 1981, 1983). It has been modified to be fully three-dimensional, and to allow for temperature dependent power law rheology and buoyancy forces. It simulates viscoelastic deformation described by a Maxwell body, for which the following constitutive equation holds:

$$\partial\varepsilon/\partial t = \sigma/2\mu + 1/E\partial\sigma/\partial t \quad (1)$$

where ε is strain, μ is dynamic viscosity, σ is stress, t is time and E is Young's modulus. In some of the tests, the slippery nodes technique (Melosh and Williams, 1989) is used along a specified transform fault. In such models the fault plane is represented by a vertical internal surface with zero resolved shear stress, and the fault plane is oriented perpendicular to the spreading axes. This is a simplified description, and transform fault systems are clearly more complicated than this.

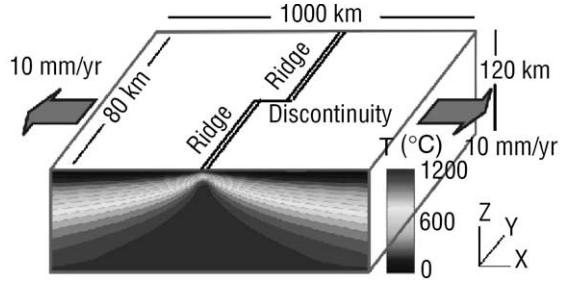

Fig. 2. Modeling setup and a profile of the temperature field result. Two (half) ridge segments are offset at a discontinuity (y=40 km). Ridge offset can vary and can either be transform fault (with variable slip allowed along specified plane) or non-transform (distributed deformation is calculated). Basaltic upper crust (3 km thick) overlies gabbro lower crust (3 km thick) (Tables 1 and 2). Mantle part has a peridotite composition. A constant temperature of 0 °C is prescribed at the surface and 1333 °C at the base, zero heat flow boundary conditions are prescribed through sides. Back and front sides are kept fixed in the y-direction and free to move in x- and z-directions. Base of model is horizontal, but free slip, top surface free to move in all directions.

However, for reasons of computational complexity we have assumed this simplified geometry. The state of stress is constrained by the force balance

$$\partial\sigma_{ij}/\partial x_j + \rho g_i = 0 \tag{2}$$

in which g is gravity, ρ is density, and i, j vary 1–3 for x, y and z directions. In our simulations density follows a linear equation of state and only thermal buoyancy is considered:

$$\rho = \rho_0(1 - \alpha T) \tag{3}$$

Here, α is the thermal expansion coefficient and T is temperature. Thermal expansion is believed to be the largest source of density gradients in the mantle beneath spreading centers. The mechanical part is coupled to a thermal finite element routine based on Greenough and Robinson (2000). The temperature field is calculated using the heat flow equation

$$\rho c_p \mathrm{d}T/\mathrm{d}t = \partial_j k \partial_j T + H \tag{4}$$

in which ρ is defined by Eq. (3), c_p is specific heat, k is conductivity and H is heat production in the crust, taken to be zero in these oceanic lithosphere simulations. The heat flow equation is solved every time step on the same grid as the displacement field in the mechanical part of the code. The Lagrangian formulation is used, so the material is attached to the nodal points. The mechanical and thermal parts are coupled through the temperature dependent power law rheology and buoyancy forces, while advection of heat is accounted for by the nodal displacements. The relationship between stress and strain rate (e) is described by

$$e = A\sigma^n \exp(-Q/RT) \tag{5}$$

where A is a material constant, n is the power law exponent, Q is activation energy and R is the gas constant. Eqs. (1)–(5) are solved using the finite element method, whereby the time step size is calculated according to the Courant criterion. As we are interested in studying the final "steady state" regime for a particular model geometry, numerical experiments were run for about 3 My. This period was long enough for a steady state regime to be achieved, without large distortions of the numerical grid.

Melt production is computed but not yet tied to model evolution in these initial runs through, for example, density effects. Decompressional partial melting of the mantle due to plate separation is calculated using the empirical expressions by McKenzie and Bickle (1988) to determine the melt fraction of a rock. Empirical relations for mantle peridotite are used for the liquidus (McKenzie and Bickle, 1988) and solidus (Hirschmann, 2000). We use 13,125 nodal points with varying spacing in the x, y and z directions. The mesh is finest near the ridges in the x-direction (about 2 km grid spacing), near the transform fault in the y-direction (about 0.6 km) and in the crustal layers (about 0.6 km grid spacing).

2.2. Model geometry, boundary conditions and rheology

The model geometry is shown in Fig. 2. Calculations are performed in a domain of $1000 \times 80 \times 120$ km ($x \times y \times z$). For the mechanical and thermal model, an initial constant crustal thickness of 6 km is assumed divided in an upper crust and lower crust of equal thickness. In some tests (Table 1), crustal thickness is varied along-strike; decreasing either gradually or step-

Table 1
Model geometries discussed in the text

Test	Offset length (km)	Nature	Crustal thickness
Test A	30	Non-transform	Constant
Test B	20	Non-transform	Constant
Test C	30	Non-transform	Decreasing gradually[a]
Test D	30	Non-transform	Decreasing abrupt[b]
Test E	30	Transform	Constant
Test F	100	Transform	Constant

[a] Linear decrease in crustal thickness from segment center toward segment-end from 6 to 4 km.
[b] Sharp decrease in crustal thickness at distance of 10 km from segment-end from 6 to 4 km, and constant crustal thickness between segment center and distance of 10 km from segment-end.

wise toward the segment-end from a total thickness of 6 to 4 km (with a 2 km thick upper crust and 2 km thick lower crust). The rest of the domain is assumed to be mantle material. Crustal rheology is based on a basaltic composition overlying a gabbro layer (see Table 2, for rheological parameters). A peridotite composition and corresponding rheology is adopted for the mantle part of the domain.

In this study we simulate a magmatic accretionary stage, and assume that all extensional strain is accommodated by axial magmatism in the rift valley, which means in the context of our modeling that the axial region is specified by a small zone of limited elastic strength (Young's modulus is $1 \cdot 10^8$ Pa). The relative ease of deformation in the axial zone keeps stress from building up; this is intended to simulate stress reductions that would accompany axial magmatic intrusion. The elements in the axial zone are allowed to widen according to the stresses or forces acting upon them; there is no limitation to the widening rate. This simulation of the axial zone differs from the approach chosen by Buck et al. (2005), who have prescribed elements in the axial zone that are made to widen at a constant (limited) rate. The treatment of the axial valley in the numerical model determines to a large extent the predicted deformation of the young oceanic lithosphere, this will be discussed in Section 3.3. With our approach, plate rifting is concentrated within the axial zone and the inside and outside corner plates spread independently. The location of rifting is allowed to evolve during the dynamic evolution.

The nature of the ridge discontinuity and offset distance are varied between different models: we tested both first and second-order discontinuities of different lengths (Table 1). First order discontinuities are simulated by deformation along a transform fault using the slippery nodes approach (Melosh and Williams, 1989). The transform fault is placed in the initial setup perpendicular to the ridge segments, and extends to 12 km depth, or twice the crustal thickness. Tele-seismic and micro-earthquake studies indicate brittle rupture at depths of 10–12 km near segment ends (Bergman and Solomon, 1990; Kong et al., 1992). Deformation for the transform and non-transform discontinuity tests is allowed to develop as required by boundary conditions and material properties.

Gravity anomalies and seismic refraction studies suggest the crust may be thinned up to 3 km near transforms (Purdy and Detrick, 1986; Lin et al., 1990; Tolstoy et al., 1993). We choose 2 scenarios to illustrate the possible effect that along-strike changes in crustal thickness (and therefore the strength of the overall lithosphere) might have on the deformation. The first model assumes that thickness decreases linearly from segment center to the end (Model C, see below); the second model has constant crust up until 10 km from the end of the segment, then rapid thinning occurs into the discontinuity (Model D).

For the thermal model, an oceanic lithosphere geotherm varying with the square-root of plate age is prescribed initially for the mantle part of the domain and a linear temperature profile for the crust. Hereby the plate age is in accordance with velocity boundary conditions. Lower initial temperatures are used for the crust as an approximation for hydrothermal cooling, no further effect is included during model evolution. A constant temperature of 0 °C is adopted for the surface and 1333 °C for the base of the domain (120 km depth). Through the sides of the model a zero heat flow boundary condition is prescribed. For the mechanical model, plate velocity boundary conditions are applied parallel to the x-direction on the left and right sides, with a total spreading rate of 20 mm/yr. The back and front sides are kept fixed in the y-direction (appropriate as long as the y boundaries are distant from regions of main interest such as the discontinuity, and along-strike flow is significantly less than across-strike flow) and free to move in the x- and z-directions. The base of the model is held horizontal but free to move in the x-direction and the top surface is free to move in all directions. The size of the model domain was chosen to be large enough so that the base and sides are far enough away from the melting zone and locus of our interest, and boundary conditions allow full development of an upwelling zone. A different choice of boundary conditions at the base would not influence the results significantly in the shallow region of our focus.

Table 2
Material parameter values (Turcotte and Schubert, 2002)

	Basalt	Gabbro	Peridotite
Density	2800	2950	3350
Young's modulus	$8 \cdot 10^{10}$	$8 \cdot 10^{10}$	$1 \cdot 10^{10}$
Poisson's ratio	0.25	0.2	0.28
Power law exponent, n	3.0	3.0	3.0
Activation energy, Q	186.5	186.5	555
Material constant, A	$3.16 \cdot 10^{-26}$	$3.16 \cdot 10^{-26}$	$7.0 \cdot 10^{-14}$
Conductivity	2.6	2.6	3.1
Specific heat	1050	1050	1050
Thermal expansion	$1 \cdot 10^{-5}$	$1 \cdot 10^{-5}$	$1 \cdot 10^{-5}$

Density [kg m^{-3}], Young's modulus [Pa], activation energy [kJ $mole^{-1}$], material constant [Pa^{-n} s^{-1}], conductivity [Wm^{-1} K^{-1}], specific heat [Jkg^{-1} K^{-1}], thermal expansion [K^{-1}].

3. Modeling results

Results from 6 tests of coupled thermo-mechanical evolution associated with offset spreading plate boundaries are presented below. Between the experiments, offset length, nature of the offset, and along-axis crustal thickness were varied. Model A is the "standard" test, with a non-transform, 30 km offset and constant crustal thickness. In model B the offset length is different from test A; 20 km, and in models C and D the crustal thickness decreases gradually and abruptly, respectively, toward the segment ends. Model E differs from model A in that the discontinuity is now a transform fault, and in model F the offset of the transform discontinuity is increased to 100 km. The effect on temperature structure and decompressional partial melting, flow field of the lithosphere and mantle, and stress field are described.

3.1. Thermal structure, melt generation and mantle flow

In general, the predicted thermal structure, melt production, and basic flow agree with that found by previous workers (Fig. 3, and e.g., Phipps Morgan and Forsyth, 1988; Shen and Forsyth, 1992; Rabinowicz et al., 1993). Fig. 3C shows the depth of the 400 °C isotherm, which is used here as a first order estimation

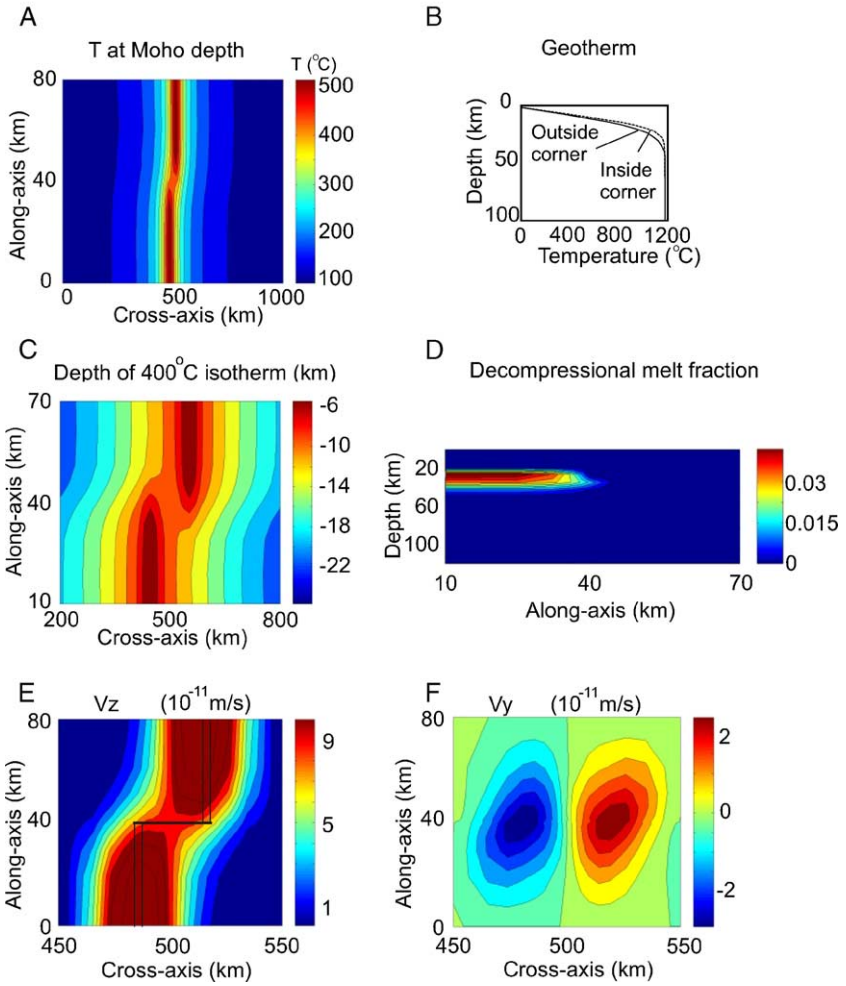

Fig. 3. A) and B): Final results for model A (3 My). A) Map view of predicted temperature field at Moho depth (6 km). Age of the plates increases from 0 My at the ridge to about 50 My at the sides of the model domain. B) Geotherm at inside and outside corners (~12 km from axis, ~5 km from discontinuity). Inside corners are found to be warmer than outside corners in all models that we tested. C) Depth of 400 °C isotherm, as a first-order estimation of the brittle to ductile transition in oceanic lithosphere, Model F. D) Decompressional melt fraction, Model F. This is a vertical transect through the western ridge. E) Model A. Vertical component of velocity field (upwelling), map view at 20 km depth. F) Model A. Ridge parallel, horizontal component of velocity field, map view at 20 km depth.

of the brittle to ductile transition. As expected, the depth of this isotherm increases toward the ridge offset. At inside corners the brittle to ductile transition is predicted at shallower depths than at outside corners. At Moho depth, temperatures below the spreading ridge are predicted to be below temperatures associated with the brittle to ductile transition, consistent with axial seismic activity beneath the Mid-Atlantic Ridge extending to depths of 6 to 10 km (Huang and Solomon, 1988; Toomey et al., 1988). A comparison of the standard model results with the predicted thermal structures of the other 5 models shows, as expected, that a decrease (increase) in offset length is accompanied by less (more) cooling of the lithosphere toward the segment-end. In all models, significant along-axis differences in temperature, with relative highs up to ~80 °C focused near the ridge offsets, exist; axial thermal regimes are colder near discontinuities. In all tests, inside corners are warmer than outside corners (Fig. 3B). This difference may be as large as 100 °C at 20 km depth. There is no detectable difference between thermal structures predicted for models A and E (30 km offset, non-transform discontinuity versus 30 km transform discontinuity). Also the effect of along-axis initial crustal thickness variations (either gradually or abruptly thinned toward the segment end, Table 1) on the temperature structure is limited. Both models C and D predict temperatures to be slightly higher at the segment-end than in the standard test.

In the standard test, base lithosphere depth (here taken at 1000 °C) varies from ~21.5 km below the spreading center near the discontinuity to ~13 km below the ridge at a distance of 20 km from the discontinuity. Thus, toward the center of ridge segments, the axial regime is predicted to be warmer, and the axial lithosphere thinner. This implies that oceanic lithosphere is stronger near discontinuities than near segment centers. Rifting of older oceanic lithosphere is thus expected to occur away from segment-ends. This has been observed in magnetic anomaly patterns, for example the breakup of the Farallon and Vancouver Plates, 55 Ma (Atwater, 1989).

Thickening of the axial lithosphere near segment-ends is expected to result in a smaller degree of melting near the discontinuity. The melt fraction is predicted to be smaller toward the segment-end, consistent with lower temperatures there (Fig. 3D). This result fits with the observation that basalts originating from closer to transform faults are probably produced by smaller degrees of mantle melting than basalts originating from segment centers (Ghose et al., 1996; Niu and Batiza, 1994; Langmuir and Bender, 1984). The simulations predict a reduction in melt generation closer to the discontinuity, however, melt production is not absent at the ridge-end. The depth at which melting commences is rather constant over the ridge-axis, only the cessation of mantle melting is at greater depths closer to the discontinuity, in line with earlier studies (e.g., Ghose et al., 1996). Distribution of melt fraction appears to be dependent on offset length; the melt fraction near the discontinuity is less reduced with respect to a segment center when the offset is smaller. Specified along-axis crustal thickness variations (that are at present not directly tied to melt production in our models) influence, in turn, the melt fraction to some extent; in accordance with the slightly higher temperatures near the segment-ends, melt fractions are somewhat less reduced near the discontinuity for models C and D. The model simulations predict that distribution of melt fraction is not dependent on nature of the discontinuity. This is consistent with the negligible effect of the nature of the discontinuity on the thermal field.

The upwelling and ridge–parallel flow patterns (Fig. 3E, F) are predicted to depend on offset length as shown by previous workers (e.g., Shen and Forsyth, 1992). The nature of the offset (transform versus non-transform) and along-axis variations in crustal thickness are not found to have an important effect on upwelling; neither amplitude nor shape of the contours are significantly modified. Fig. 3F shows the along-axis horizontal flow on the same horizontal section as Fig. 3E, also for the standard test. Material flows toward the spreading axes from beneath the older plate opposite of the discontinuity. An explanation given by Shen and Forsyth (1992) for this flow is that part of the material that is dragged away from the spreading axes is supplied in this way. The model simulations predict that there exists a deficit in upwelling below the axis near the ridge truncation and excessive upwelling beyond the ridge end, which results in a north–south (or south–north for the eastern ridge) direction of material transport.

3.2. Shape and location of the plate boundary

The axis-perpendicular velocity component is shown in Fig. 4. The map view in Fig. 4A for the standard non-transform, 30 km offset model, at the top surface of the model domain (seafloor), shows a coherent movement of the plates away from the spreading ridge segments. In Fig. 4B a detailed view shows the wide, oblique zone of deformation of the non-transform discontinuity between the two ridge tips. The second-order

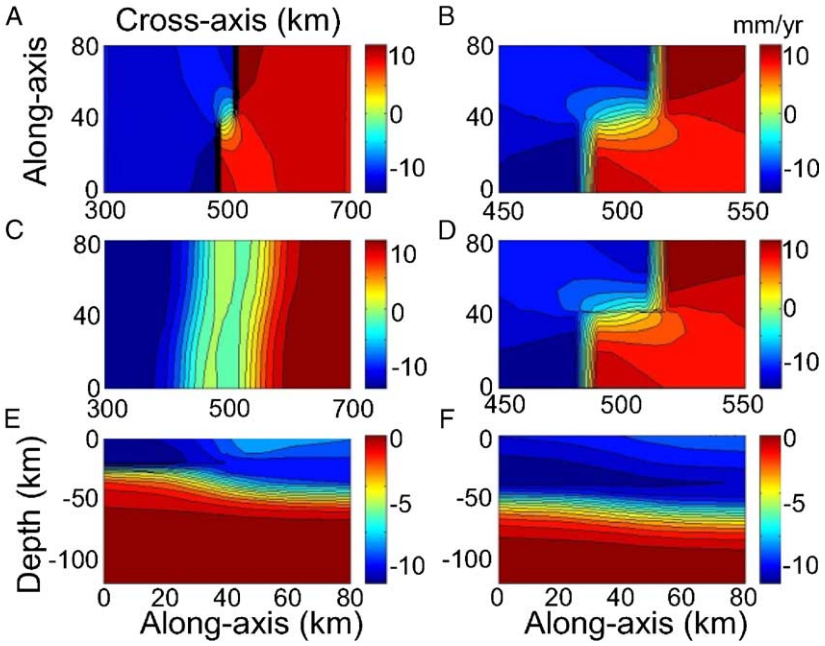

Fig. 4. Ridge–perpendicular horizontal component of velocity field (v_x) after 3 My of evolution. A) Map view at top-surface of model domain for test A. The eastern plate moves toward the positive x-direction, the western plate moves toward the negative x-direction. B) Same, detail of A). The non-transform discontinuity rotates to become more parallel to the ridge axes. C) Same scale as A), but at depth of 55 km. What is left of the discontinuity at this depth is a bend in the flow field. D) Same detail as B), but for test E. The transform discontinuity remains parallel to the spreading direction. E) Vertical transect parallel to ridge, 12 km west of western ridge for test A. F) Same as E), but 45 km west of western ridge. See text for discussion.

discontinuity tends to change its orientation with time to become more parallel to the ridges and more perpendicular to the plate spreading direction. This contrasts with a first-order or transform discontinuity, where initial orientation is maintained in time (Fig. 4D). Prior modeling studies (Grindlay and Fox, 1993) predict that smaller offset lengths than tested in the present study may be needed to maintain the geometry. The sharp surface discontinuity transitions downward to a bend in the flow pattern by 55 km depth (Fig. 4C). Fig. 4E and F are vertical transects parallel to and just left of the western ridge. The model predicts a gradient in this component of the velocity field close to the ridge (light blue colored part in crust). Deformation associated with the discontinuity extends to the outside corners of the ridge–offset setting. Between all the tests performed, differences in the spreading parallel component of the velocity field are largest between the transform and non-transform tests. Along-axis crustal thickness variations do not modify the flow pattern or amplitudes significantly, which is also the case for different offset lengths.

The boundary between inside and outside corner plates remains vertical in the center of the offset but

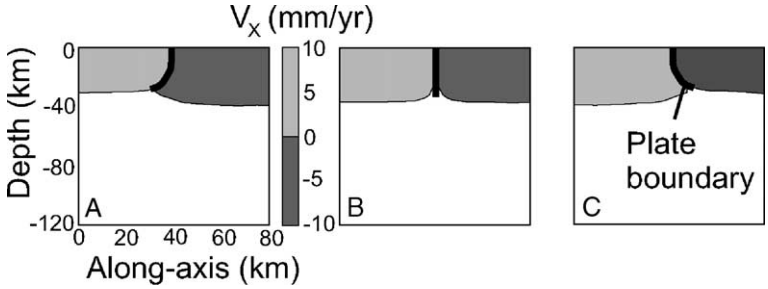

Fig. 5. Vertical transects parallel to ridges, through transform fault, showing plate boundary (where ridge–perpendicular component of velocity field changes direction, thick black lines). A) 8 km from western ridge, B) through center of transform fault, C) 8 km from eastern ridge. The plate boundary is found to be curved in the inside corners and vertical below the center of the transform fault.

is curved in the inside corners near the ridge–transform intersection (Fig. 5A–C). This is predicted for both transform and non-transform discontinuities. The older and thicker plate seems to drag away some of the material from beneath the opposite plate. The curve is strongest near the ridge–offset intersection and gradually reduces along axis toward the segment center. The older plate may extend as much as 10 km beneath the younger plate near the intersection, and it transitions to being vertical at a distance of about 30 km from the offset. This distance changes somewhat between different tests; it is clearly smaller with smaller offsets, and thus seems to be offset-length dependent. The main difference between transform- and non-transform discontinuity tests is the shape of the curve at shallow depths (seafloor); the model does not predict clear differences below the transform depth. These interpretations differ somewhat from earlier findings (Furlong et al., 2001) due to different model assumptions and treatment of the ridge-axis. The non-transform initial configuration is not maintained in time at the surface (seafloor), see also Fig. 4, in contrast to the transform configuration. The presence of older and thicker oceanic lithosphere from opposite of the discontinuity below the end of the ridge segment, especially when offset lengths are larger, is expected to make it more difficult for mantle material to rise to the ridge ends. This could ultimately result in a ridge end that is no longer in a magmatic spreading phase. Furlong et al. (2001) suggest that such a curvature in the plate boundary beneath the segment-end might eventually result in the formation of a new, short ridge segment.

While the model results suggest that the transform plate boundary remains oriented according to the spreading direction, the non-transform discontinuity orientation changes to become more perpendicular to the spreading direction. The transform plate boundary is predicted to be a stable boundary and will only change upon changes in external factors; the non-transform discontinuity is intrinsically unstable.

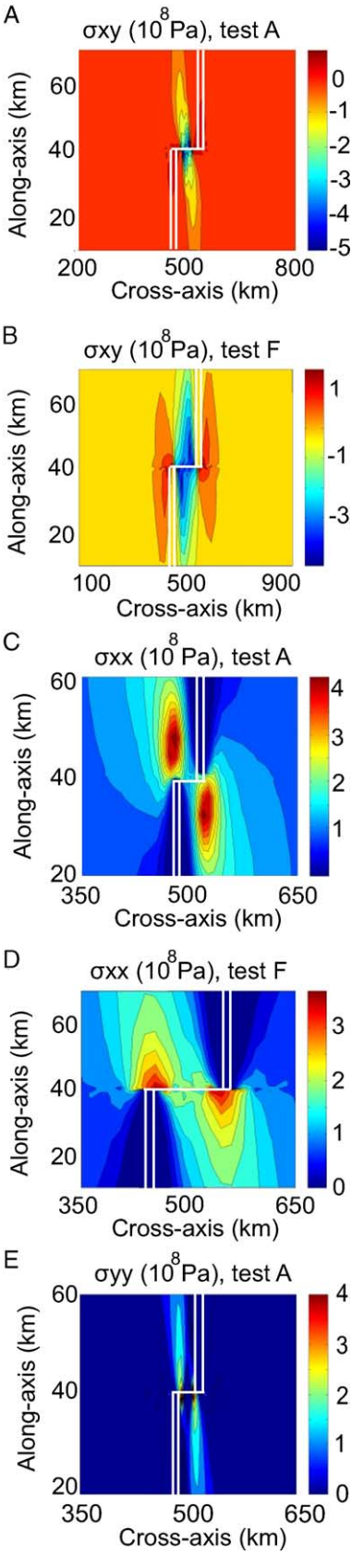

Fig. 6. Map view of predicted stress fields. The initial ridge–discontinuity–ridge configuration is sketched in each panel (double white lines), this plate boundary changes with time for model A. A) Horizontal shear stresses in crust for model A, non-transform, 30 km offset. B) Horizontal shear stresses in crust for model F, with a 100 km transform offset. Highest values are found along the transform zone and in the inside corners, but shear stresses also concentrate at outside corners. C) Ridge–perpendicular horizontal deviatoric stress field (σ_{xx}) in upper crust, model A, showing concentration of extensional stresses about 10 km offset from ridge tips. D) Same, for test F. Extensional stresses concentrate near the ridge tips. E) Ridge–parallel horizontal stress field (σ_{yy}) in upper crust, model A.

3.3. Stress field predictions and locations of crustal thinning

A map view of horizontal shear stresses in the crust is shown in Fig. 6A for model A, and in Fig. 6B for model F, with a 100 km offset, transform fault discontinuity. Highest values of shear stresses are predicted at inside corners and along the discontinuity. High amplitudes are basically confined to a small zone parallel to the ridge, and they decrease toward a segment center. It is interesting to note that shear stresses also concentrate at outside corners, but with much smaller amplitudes. The influence of the discontinuity clearly extends beyond the ridge; lithosphere deformation related to the offset is perceptible in outside corners. This pattern in the stress field can be found in all models. Stress predictions of 3-D boundary element models (Blackman, 1997; Behn et al., 2002) are in line with these results and predict shear stresses in the inside corners. Extensional (ridge normal) stresses (σ_{xx}) concentrate in line with the spreading axes near the ridge-tips (Fig. 6C and D), but high values are absent in the inside corners during the magmatic accretionary period that our model simulates. These predictions differ somewhat from results from Buck et al. (2005), who predict under certain circumstances extensional deformation in the inside corners during magmatic spreading periods. As divergent plate movement is fully accommodated by magma supply to the axial valley in our models, the inside corner lithosphere outside the axial valley is not under extension. We find largest σ_{xx} amplitudes directly adjacent to the axes for the transform discontinuity tests and some distance away (about 10 km) from the tips for the non-transform discontinuity tests. So, the ridge segments influence the adjacent lithosphere on the opposite side of the discontinuity over a distance of several tens of km. The large extensional stress amplitudes near ridge tips probably arise from the fact that plate segments on both sides of the discontinuity are coupled; either throughout the whole lithosphere (non-transform) or mainly at larger depths (transform) below the fault plane. This coupled system causes the older plate to "feel" the divergent plate separation on the other side of the discontinuity. Ridge–parallel extensional stress amplitudes (σ_{yy}) of comparable size as ridge–normal tensional stress amplitudes are predicted in a more or less ridge–parallel pattern for both transform and non-transform models (Fig. 6E), with higher values toward the ridge ends. The results do not show a concentration of high σ_{yy} values near the discontinuity or along old traces of the discontinuity.

Young oceanic lithosphere that experiences large extensional stresses is expected to deform and thin. Our experiments suggest that crustal thinning during magmatic extension concentrates in line with the spreading centers at the opposite side of the discontinuity (Fig. 7). In the case of a non-transform discontinuity, not only the regions in line with the axes where extensional stress amplitudes are highest experience thinning, but also the oblique deformed zone that continues to be under extensional stress. Also in the transform discontinuity tests some thinning near the strong transform fault is predicted. Extensional structures expressed as oceanic rift basins have been documented at both first and second-order discontinuities, for example along the slow to intermediate spreading South Atlantic Ridge (Grindlay et al., 1991). Grindlay et al. (1991) have recognized different structural geometries of second-order discontinuities. The offset length between the ridge segments appears to be a factor that influences the structural style of the discontinuity. For example, ridge parallel basins are found when offsets are small, and extensional basins that are oblique to the direction of spreading are found when offsets are large

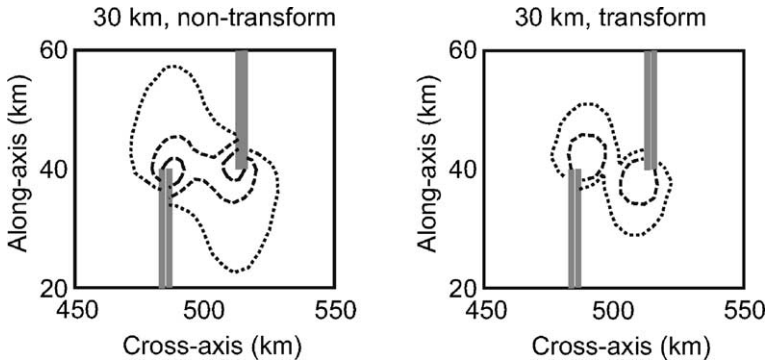

Fig. 7. Crustal thinning predicted for 30 km non-transform experiment (left panel) and 30 km offset transform test (right panel). The crustal thinning factors are defined here as the ratio between the initial crustal thickness and its present thickness. Increasing dash-lengths denote increasing amount of crustal thinning (ranging from 1.02 to 1.1).

(25–30 km; Grindlay et al., 1991). Such oblique extensional structures resemble somewhat the crustal thinning patterns predicted by the 20 and 30 km non-transform model experiments.

This suite of experiments is not intended to simulate a number of geological complexities that must also contribute to the actual deformation near ridge–discontinuities, such as formation of (detachment) faults and (flexural) uplift. Instead, we have focused on results for a reference model for which the only contributor is 3-D plate boundary geometry, which is the starting point from which subsequently added complexities can be compared. In the next section we discuss some geologically relevant aspects of our initial results.

4. Expressions of extensional deformation of (relatively young) oceanic lithosphere

Under normal conditions, the extensional stress field in young oceanic lithosphere is ridge–normal within about 20 km from the spreading axes, as indicated by earthquake focal mechanisms and observations of active normal faulting (Escartín et al., 1999; Huang and Solomon, 1988). These tensile stresses are attributed to so-called ridge-resistance arising from a stress deficiency at the ridge axis relative to the state of stress of the nearby lithosphere (e.g., Lachenbruch, 1973; Tapponnier and Francheteau, 1978). Away from the ridge axis in young oceanic lithosphere, earthquake focal mechanisms show normal faulting events with tensile axes parallel to the spreading axis (Bergman and Solomon, 1984; Reinecker et al., 2003), indicating the existence of a ridge–parallel tensile stress pattern. Explanations for this stress pattern include cooling and contraction of the lithosphere (Turcotte and Oxburgh, 1973), plate boundary forces (Cloetingh and Wortel, 1986), and changes in spreading direction (Menard and Atwater, 1968). Near ridge axis discontinuities we find the stress field to be more complex, perturbed by the discontinuity and variations in crustal and lithosphere thickness. In addition, the stress field may be modified by variations in magma production near the ridge end, a factor that was not included in this first phase of our modeling. The predicted stress fields are characterized by 1) high shear stress values in the inside corners, 2) high ridge–normal extensional stresses in line with the truncated ridge on the opposite side of the discontinuity, and 3) high transform-normal extensional stresses in a parallel pattern to the ridges.

The shear stress pattern reflects the observed anomalous faulting mechanisms along the discontinuity and near the ridge–offset intersection with respect to the otherwise ridge–normal extensional stress field. The pattern of axis-perpendicular tensile stresses in line with the ridge tips may reflect an attempt to ridge propagation during a magmatic accretionary phase. In order for a ridge to propagate, extensional stresses near the ridge tip have to overcome the strength of the lithospheric plate opposite of the discontinuity (Phipps Morgan and Parmentier, 1984). This is more likely to occur when the age-offset is small and the lithosphere adjacent to the ridge tip is relatively young and weak, when extensional stresses are larger, i.e., in case of a non-transform or strong transform discontinuity, or when spreading velocities are low, so that there is sufficient time to locally weaken lithosphere that is adjacent to the warmer ridge tip. We speculate that when extensional stresses are sufficient to thin the crust and mantle lithosphere, mantle upwelling and melting below this region will increase, resulting in segment lengthening. Other factors that have been suggested to affect ridge propagation include along-axis variations in seafloor topography, asthenospheric flow and crustal thickness (Phipps Morgan and Parmentier, 1984; West et al., 1999; Spence and Turcotte, 1985). Alternatively, Beutel (in press) has suggested that these extensional stresses might under certain circumstances result in formation of hotspot seamounts. Several studies have documented seamounts near ridge–discontinuities (e.g., Graham et al., 1999; Hekinian et al., 1999; Johnson et al., 2000; Klingelhöfer et al., 2001) that seem to have been formed near a ridge-tip. Whether the extensional stresses induced by the discontinuity are released by segment lengthening or other extensional structures is probably dependent on several factors including mantle flow patterns and thermal regime below the ridge axis (Beutel, in press), characteristics of the discontinuity, and rheology of the adjacent lithosphere. However, further modeling is required to fully test the ideas on extensional stress release.

Oceanic core complexes or mega-mullions are extensional structures, found near discontinuities or fossil traces of discontinuities, mainly in inside corners. Necessary for OCC development is the development of a large offset normal fault or a detachment fault. It takes effective localization of deformation over longer periods of time in an extensional regime to form a detachment fault system. It has been suggested that detachment fault formation is facilitated by a rheological boundary within the brittle lithosphere (Escartín et al., 2003), that the brittle–plastic transition itself functions as a rheological boundary (e.g., Davis and Lister, 1988; Brun et al., 1994; Gartrell, 1997; Tucholke et al.,

2001), that a melt-rich zone within the lithosphere guides localization of deformation (Lister and Baldwin, 1993; Parsons and Thompson, 1993; Dick et al., 2000), or that sub-horizontal regions of high shear strains resulting from the complex ridge–transform plate boundary could act as a detachment surface (Furlong et al., 2001). Although the two spreading plates are predicted to be in an overall ridge–normal extensional regime in our modeling results, high magnitude ridge–normal extensional stresses are absent in inside corners during the magmatic accretionary stage that we have simulated. The ridge–parallel tensional stress pattern suggests that the evolution of the rift mountains may be affected, and a tendency for spreading-parallel scarps to develop may occur near the discontinuity. Observations of steep scarps associated with megamullion or OCC structures suggest that both spreading axis perpendicular and parallel orientations occur, although the axis parallel orientation seems to be more common. For example, fault scarps on the Atlantis Bank (SW Indian Ridge, Baines et al., 2003) are parallel to the transform zone, but fault scarps in the Parece Vela backarc basin, northwestern Pacific (Ohara et al., 2001) appear to be parallel to the ridge axis. On other OCC structures, like the FUJI Dome, the orientation of the fault scarp seems to change direction from one part of the structure to the other (Searle et al., 2003).

This set of models illustrates that during magmatic spreading phases, extensional deformation is not predicted in the inside corner under the tested rheology and boundary conditions. Additional factors are required for inside corner formation of oceanic core complexes; the predicted stress patterns would not lead to (spreading-parallel) normal faulting in inside corners.

5. Summary

We studied 3-D effects on deformation of relatively young oceanic lithosphere near slow spreading ridge discontinuities resulting from plate boundary geometry. The chosen axial properties in the numerical model represent a slow spreading ridge during a magmatic accretionary period, during which the axial properties are not varied along-axis or in time. This set of experiments illustrates that plate boundary geometry alone contributes to variability in deformation near ridge offsets. The thermal structure predicted by our modeling is similar to results from prior models of mantle flow beneath the oceanic lithosphere. In agreement with prior studies, our model predicts that inside corners are systematically warmer than outside corners (up to 100 °C at 20 km depth), implying that the lithosphere is thinner and the brittle-to-ductile transition is positioned at shallower depth at inside corners. Below the spreading axis, base–lithosphere depth is predicted to increase from the segment center toward the segment end (from about 13 km depth to about 21.5 km depth), and oceanic lithosphere is expected to be strongest near ridge discontinuities. Decompressional partial melt generation is reduced toward the ridge discontinuity. Different geometrical setups of the discontinuity and along-axis thickness of the crust result in differences in the cessation of melting while the depth at which mantle melting commences is not significantly altered. Along-axis variations in crustal thickness influence the thermal regime and decompressional melting to some extent, but seem to have no first order effect on mantle flow.

In the models, the plate boundary between inside corner and outside corner plates is allowed to evolve and deform. This results in a curved plate boundary below the inside corners, where the opposite older and stronger plate extends for about 10 km below the younger plate. The older plate drags away material below the inside corner over a distance of up to several tens of km away from the discontinuity or ridge end, whereby the distance is dependent on offset length. Another result of plate boundary evolution in the models is that experiments show a changing orientation of non-transform discontinuities in time. The second-order discontinuity becomes more perpendicular to the spreading direction, and is found to be intrinsically unstable. The transform plate boundary is predicted to be stable and will only change upon changes in external factors, such as changes in the pole of opening, etc. The models show significant extensional deformation and crustal thinning in the oblique non-transform discontinuity zone. Results of our rather large non-transform offset experiments are fairly similar to observed oceanic rift basin structures at comparable age offset discontinuities in the Mid-Atlantic Ridge.

Ridge–normal tensile stresses concentrate in line with the ridge tip in the older plate opposite from the discontinuity and are absent in the inside corners during the accretionary phase simulated by our models. The influence of the truncated ridge may be present over a distance of several tens of km in the opposite adjacent lithosphere. The absence of tensile stresses in inside corners in our experiments suggests that it is unlikely that inside corner oceanic core complexes, which are extensional structures, are formed during magmatic spreading phases under the tested boundary conditions and rheology.

Acknowledgements

We would like to thank the reviewers for their constructive comments. This study was funded in part by NSF grant OCE-971264 and the James G. Scripps Endowment match to EAR-0105896.

References

Atwater, T., 1989. Plate tectonic history of the northeast Pacific and western North America. In: Winterer, E.L., et al. (Eds.), The Geology of North America, vol. N., pp. 21–72. Boulder, Colorado.

Baines, A.G., Cheadle, M.J., Dick, H.J.B., et al., 2003. A mechanism for the anomalous uplift of oceanic core complexes: Atlantis Bank, SW Indian Ridge. Geology 31, 1105–1108.

Behn, M.D., Lin, J., Zuber, M.T., 2002. Evidence for weak oceanic transform faults. Geophys. Res. Lett. 29. doi:10.1029/2002GL015612.

Bergman, E.A., Solomon, S.C., 1984. Source mechanisms of earthquakes near mid-ocean ridges from body waveform inversion: implications for the early evolution of oceanic lithosphere. J. Geophys. Res. 89, 11415–11441.

Bergman, E.A., Solomon, S.C., 1990. Earthquake swarms on the Mid-Atlantic Ridge: products of magmatism or extensional tectonics? J. Geophys. Res. 95, 4943–4965.

Beutel, E.K., in press. Stress induced seamount formation at ridge–transform intersections. In: Plates, plumes and paradigms, G.R. Foulger, J.H. Natland, D.C. Presnall, D.L. Anderson, (Eds.), GSA Special Paper 338.

Blackman, D.K., 1997. Variation in lithospheric stress along ridge–transform plate boundaries. Geophys. Res. Lett. 24, 461–464.

Blackman, D.K., Cann, J.R., Janssen, B., Smith, D., 1998. Origin of extensional core complexes: evidence from the Mid-Atlantic Ridge at Atlantis Fracture Zone. J. Geophys. Res. 103, 21315–21333.

Blackman, D.K., Karson, J.A., Kelley, D.S., et al., 2002. Geology of the Atlantis Massif (Mid-Atlantic Ridge, 30°N): implications for the evolution of an ultramafic oceanic core complex. Mar. Geophys. Res. 23, 443–469.

Brun, J.-P., Sokoutis, D., van den Driessche, J., 1994. Analogue modeling of detachment fault systems and core complexes. Geology 22, 319–322.

Buck, W.R., Lavier, L.L., Poliakov, A.N.B., 2005. Modes of faulting at mid-ocean ridges. Nature 434, 719–723.

Cann, J.R., Blackman, D.K., Smith, D.K., McAllister, E., Janssen, B., Mello, S., Avgerinos, E., Pascoe, A.R., Escartín, J., 1997. Corrugated slip surfaces formed at ridge–transform intersections on the Mid-Atlantic Ridge. Nature 385, 329–332.

Carbotte, S., Welch, S.M., MacDonald, K.C., 1991. Spreading rates, rift propagation, and fracture zone offset histories during the past 5 My on the Mid-Atlantic Ridge; 25°–27°30'S and 31°–34°30'S. Mar. Geophys. Res. 13, 51–80.

Cloetingh, S.A.P.L., Wortel, R., 1986. Stress in the Indo–Australian plate. Tectonophysics 132, 49–67.

Davis, G.A., Lister, G.S., 1988. Detachment faulting in continental extension: perspectives from the southwestern U.S. Cordillera. Geol. Soc. Amer., Spec. Pap. 218, 133–159.

Dick, H.J.B., Bryan, W.B., Thompson, G., 1981. Low-angle faulting and steady-state emplacement of plutonic rocks at ridge–transform intersections. Eos Trans. AGU 62, 406.

Dick, H.J.B., Meyer, P.S., Bloomer, S.H., Kirby, S.H., Stakes, D.S., Mawer, C.K., 1991. Lithostratigraphic evolution of an in situ section of oceanic layer 3. In: Von Herzen, R.P., et al. (Eds.), Proc. Oc. Dr. Progr. Sci. Res., vol. 118, pp. 439–538.

Dick, H.J.B., Natland, J.H., Alt, J.C., Bach, W., Bideau, D., Gee, J.S., et al., 2000. A long in situ section of the lower ocean crust; results of ODP Leg 176 drilling at the southwest Indian Ridge. Earth Planet. Sci. Lett. 179, 31–51.

Escartín, J., Cowie, P.A., Searle, R.C., Allerton, S., Mitchell, N.C., MacLeod, C.J., Slootweg, A.P., 1999. Quantifying tectonic strain and magmatic accretion at a slow spreading ridge segment, Mid-Atlantic Ridge, 29°N. J. Geophys. Res. 104, 10421–10437.

Escartín, J., Mével, C., MacLeod, C.J., McCaig, A.M., 2003. Constraints on deformation conditions and the origin of oceanic detachments: the Mid-Atlantic Ridge core complex at 15°45'N. Geochem. Geophys. Geosyst. 4. doi:10.1029/2002GC000472.

Forsyth, D.W., Wilson, B., 1984. 3-Dimensional temperature structure of a ridge–transform–ridge system. Earth Planet. Sci. Lett. 70, 355–362.

Fujita, K., Sleep, N.H., 1978. Membrane stresses near ocean ridge–transform intersections. Tectonophysics 50, 207–221.

Furlong, K.P., Sheaffer, S.D., Malservisi, R., 2001. Thermal rheological controls on deformation within oceanic transforms. Geol. Soc. London, Spec. Publ. 186, 65–83.

Gartrell, A.P., 1997. Evolution of rift basins and low-angle detachments in multilayer analog models. Geology 25, 615–618.

Ghose, I., Cannat, M., Seyler, M., 1996. Transform fault effect on mantle melting in the MARK area (Mid-Atlantic Ridge south of the Kane Transform). Geology 24, 1139–1142.

Graham, D.W., Johnson, K.T.M., Priebe, L.D., Lupton, J.E., 1999. Hotspot–ridge interaction along the southeast Indian Ridge near Amsterdam and St. Paul Islands: helium isotope evidence. Earth Planet. Sci. Lett. 167, 297–310.

Greenough, C., Robinson, K.R., 2000. The finite element library. Release 4.0 http://www.cse.clrc.ac.uk.

Grindlay, N.R., Fox, P.J., 1993. Lithospheric stresses associated with nontransform offsets of the Mid-Atlantic Ridge: implications from a finite element analysis. Tectonics 12, 982–1003.

Grindlay, N.R., Fox, P.J., Macdonald, K.C., 1991. Second-order ridge axis discontinuities in the South Atlantic: morphology, structure, and evolution. Mar. Geophys. Res. 13, 21–49.

Hekinian, R., Stoffers, P., Ackermand, D., Revillon, S., Maia, M., Bohn, M., 1999. Ridge–hotspot interaction; the Pacific–Antarctic Ridge and the Foundation Seamounts. Mar. Geol. 160, 199–233.

Hirschmann, M.M., 2000. Mantle solidus: experimental constraints and the effects of peridotite composition. Geochem. Geophys. Geosyst. 1, 2000GC000070.

Huang, P.Y., Solomon, C.S., 1988. Centroid depths of mid-ocean ridge earthquakes: dependence on spreading rate. J. Geophys. Res. 93, 13445–13447.

Johnson, K.T.M., Graham, D.W., Rubin, K.H., Nicolaysen, K., Scheirer, D.S., Forsyth, D.W., Baker, E.T., 2000. Boomerang Seamount; the active expression of the Amsterdam–St. Paul hotspot, southeast Indian Ridge. Earth Planet. Sci. Lett. 183, 245–259.

Karson, J.A., 1990. Seafloor spreading on the Mid-Atlantic Ridge; implications for the structure of ophiolites and oceanic lithosphere produced in slow-spreading environments. In: Malpas, J., et al., (Eds.), Proc. of Symposium Troodos, vol. 1987. Geological Survey Dept., Nicosia, pp. 547–553.

Karson, J.A., Dick, H.J.B., 1983. Tectonics of ridge–transform intersections at the Kane Fracture Zone, 24°N on the Mid-Atlantic Ridge. Mar. Geophys. Res. 6, 51–98.

Klingelhöfer, F., Minshull, T.A., Blackman, D.K., Harben, P., Childers, V., 2001. Crustal structure of Ascension Island from wide-angle seismic data: implications for the formation of near-ridge volcanic islands. Earth Planet. Sci. Lett. 190, 41–56.

Kong, L.S., Solomon, S.C., Purdy, G.M., 1992. Microearthquake characteristics of a mid-ocean ridge along-axis high. J. Geophys. Res. 97, 1659–1685.

Lachenbruch, A.H., 1973. A simple mechanical model for oceanic spreading centers. J. Geophys. Res. 78, 3395–3417.

Lagabrielle, Y., Bideau, D., Cannat, M., Karson, J.A., Mevel, C., 1998. Ultramafic–mafic plutonic rock suites exposed along the Mid-Atlantic Ridge (10°N–30°N). Symmetrical–asymmetrical distribution and implications for seafloor spreading processes. In: Buck, Y., et al. (Eds.), Faulting and Magmatism at Mid-Ocean Ridges, AGU Monograph, vol. 106, pp. 153–176.

Langmuir, C.H., Bender, J.F., 1984. The geochemistry of oceanic basalts in the vicinity of transform faults: observations and implications. Earth Planet. Sci. Lett. 69, 107–124.

Lin, J., Purdy, G.M., Schouten, H., Sempéré, J.-C., Zervas, C., 1990. Evidence from gravity data for focused magmatic accretion along the Mid-Atlantic Ridge. Nature 344, 627–632.

Lister, G.S., Baldwin, S.L., 1993. Plutonism and the origin of metamorphic core complexes. Geology 21, 607–610.

Lister, G.S., Davis, G.A., 1989. The origin of metamorphic core complexes and detachment faults formed during Tertiary continental extension in the northern Colorado River region, U.S.A. J. Struct. Geol. 11, 65–94.

Lonsdale, P., 1994. Geomorphology and structural segmentation of the crest of the southern (Pacific–Antarctic) East Pacific Rise. J. Geophys. Res. 99, 4683–4702.

Macdonald, K.C., 1986. The crest of the Mid-Atlantic Ridge: models for crustal generation processes and tectonics. In: Vogt, P.R., Tucholke, B.E. (Eds.), The Geology of North America, vol. M. Geol. Soc. Am., Boulder, Colorado, pp. 51–68.

MacLeod, C.J., Escartín, J., Banerji, D., et al., 2002. First direct evidence for oceanic detachment faulting: the Mid-Atlantic Ridge, 15°45'N. Geology 30, 879–882.

McKenzie, D., Bickle, M.J., 1988. The volume and composition of melt generated by extension of the lithosphere. J. Petrol. 29, 625–679.

Melosh, H.J., Raefsky, A., 1980. The dynamical origin of subduction zone topography. Geophys. J. R. Astron. Soc. 60, 333–354.

Melosh, H.J., Raefsky, A., 1981. A simple and efficient method for introducing faults into finite element computations. Seismol. Soc. Am. Bull. 71, 1391–1400.

Melosh, H.J., Raefsky, A., 1983. Anelastic response to dip slip earthquakes. J. Geophys. Res. 88, 515–526.

Melosh, H.J., Williams, C.A., 1989. Mechanics of graben formation in crustal rocks: a finite element analysis. J. Geophys. Res. 94, 13961–13973.

Menard, H.W., Atwater, T.M., 1968. Changes in direction of sea floor spreading. Nature 219, 463–467.

Mével, C., Cannat, M., Gente, P., Marion, E., Auzende, J.M., Karson, J.A., 1991. Emplacement of deep crustal and mantle rocks on the west median valley wall of the MARK area (MAR, 23°N). Tectonophysics 190, 31–53.

Niu, Y., Batiza, R., 1994. Magmatic processes at a slow-spreading ridge segment: 26°S Mid-Atlantic Ridge. J. Geophys. Res. 99, 19719–19740.

Ohara, Y., Yoshida, T., Kato, Y., Kasuga, S., 2001. Giant megamullion in the Parece Vela backarc basin. Mar. Geophys. Res. 22, 47–61.

Parsons, T., Thompson, G.A., 1993. Does magmatism influence low-angle normal faulting? Geology 21, 247–250.

Phipps Morgan, J., Forsyth, D.W., 1988. Three-dimensional flow and temperature perturbations due to a transform offset: effects on oceanic crustal and upper mantle structure. J. Geophys. Res. 93, 2955–2966.

Phipps Morgan, J., Parmentier, E.M., 1984. Lithospheric stress near a ridge–transform intersection. Geophys. Res. Lett. 11, 113–116.

Purdy, G.M., Detrick, R.S., 1986. Crustal structure of the Mid-Atlantic Ridge at 23°N from seismic refraction studies. J. Geophys. Res. 91, 3739–3762.

Rabinowicz, M., Rouzo, S., Sempéré, J.-C., Rosemberg, C., 1993. Three-dimensional mantle flow beneath mid-ocean ridges. J. Geophys. Res. 98, 7851–7869.

Reinecker, J., Heidbach, O., Mueller, B., 2003. The 2003 Release of the World Stress Map. http://www.world-stress-map.org.

Searle, R.C., Cannat, M., Fujioka, K., Mével, C., Fujimoto, H., Bralee, A., Parson, L., 2003. FUJI Dome: a large detachment fault near 64°E on the very slow-spreading southwest Indian Ridge. Geochem. Geophys. Geosyst. 4. doi:10.1029/2003GC000519.

Sempéré, J.-C., Blondel, P., Briais, A., Fujiwara, T., Géli, L., Isezaki, N., Pariso, J.E., Parson, L., Patriat, P., Rommevaux, C., 1995. The Mid-Atlantic Ridge between 29°N and 31°30'N in the last 10 Ma. Earth Planet. Sci. Lett. 130, 45–55.

Shen, Y., Forsyth, D.W., 1992. The effects of temperature- and pressure-dependent viscosity on three-dimensional passive flow of the mantle beneath a ridge–transform system. J. Geophys. Res. 97, 19717–19728.

Smith, D.K., Escartín, J., Cannat, M., Tolstoy, M., Fox, C.G., Bohnenstiehl, D.R., Bazin, S., 2003. Spatial and temporal distribution of seismicity along the northern Mid-Atlantic Ridge (15°–35°N). J. Geophys. Res. 108. doi:10.1029/2002JB001964.

Sparks, D.W., Parmentier, E.M., Phipps Morgan, J., 1993. Three-dimensional mantle convection beneath a segmented spreading center: implications for along-axis variations in crustal thickness and gravity. J. Geophys. Res. 98, 21977–21995.

Spence, D.A., Turcotte, D.L., 1985. Magma-driven propagation of cracks. J. Geophys. Res. 90, 575–580.

Tapponnier, P., Francheteau, J., 1978. Necking of the lithosphere and the mechanics of slowly accreting plate boundaries. J. Geophys. Res. 83, 3955–3970.

Tolstoy, M., Harding, A.J., Orcutt, J.A., 1993. Crustal thickness on the Mid-Atlantic Ridge; bull's eye gravity anomalies and focused accretion. Science 262, 726–729.

Toomey, D.R., Solomon, S.C., Purdy, G.M., Murray, M.H., 1988. Microearthquakes beneath the median valley of the Mid-Atlantic Ridge near 23°N: tomography and tectonics. J. Geophys. Res. 93, 9093–9112.

Tucholke, B.E., Lin, J., 1994. A geological model for the structure of ridge segments in slow spreading ocean crust. J. Geophys. Res. 99, 11937–11958.

Tucholke, B.E., Lin, J., Kleinrock, M.C., 1998. Megamullions and mullion structure defining oceanic metamorphic core complexes on the Mid-Atlantic Ridge. J. Geophys. Res. 103, 9857–9866.

Tucholke, B.E., Fujioka, K., Ishihara, T., Hirth, G., Kinoshita, M., 2001. Submersible study of an oceanic megamullion in the central North Atlantic. J. Geophys. Res. 106, 16145–16161.

Turcotte, D.L., Oxburgh, E.R., 1973. Mid-plate tectonics. Nature 244, 337–339.

Turcotte, D.L., Schubert, G., 2002. Geodynamics, 2nd edition. Cambridge University Press. 456 pp.

Wernicke, B., 1985. Uniform-sense normal simple shear of the continental lithosphere. Can. J. Earth Sci. 22, 108–125.

Wernicke, B., 1992. Cenozoic extensional tectonics of the U.S. Cordillera. In: Burchfiel, B.C., et al. (Eds.), The Geology of North America, vol. G-3. Geol. Soc. Am., Boulder, Colorado, pp. 553–581.

Wernicke, B., 1995. Low-angle normal faults and seismicity: a review. J. Geophys. Res. 100, 20159–20174.

West, B.P., Lin, J., Christie, D.M., 1999. Forces driving ridge propagation. J. Geophys. Res. 104, 22845–22858.